JAAS

Trace Xenon Detection in Helium Environment via Laser-induced Breakdown Spectroscopy

Journal:	*Journal of Analytical Atomic Spectrometry*
Manuscript ID	JA-ART-12-2020-000513.R2
Article Type:	Paper
Date Submitted by the Author:	24-Feb-2021
Complete List of Authors:	Burger, Milos; University of Michigan, Department of Nuclear Engineering and Radiological Sciences Garrett, Londrea; University of Michigan Burak, Adam; University of Michigan Petrov, Victor; University of Michigan Manera, Annalisa; University of Michigan Sabharwall, Piyush; Idaho National Laboratory Sun, Xiaodong; University of Michigan Jovanovic, Igor; University of Michigan

Journal Name

ARTICLE TYPE

Cite this: DOI: 00.0000/xxxxxxxxxx

Trace Xenon Detection in Helium Environment via Laser-induced Breakdown Spectroscopy

M. Burger,*[a,b] L. Garrett,[a,b] A. J. Burak,[a] V. Petrov,[a] A. Manera,[a] P. Sabharwall,[c] X. Sun[a] and I. Jovanovic[a,b]

Received Date
Accepted Date

DOI: 00.0000/xxxxxxxxxx

There is significant motivation to develop and deploy novel nuclear reactor designs to deliver improved performance, safety, and economics for nuclear energy. In gas-cooled fast reactors that use helium as the primary coolant, the presence of xenon could indicate the onset of the fuel failure. We performed a feasibility study using single-pulse laser-induced breakdown spectroscopy to assess the sensitivity for trace xenon detection in a helium buffer of the pressure of 1.25 bar at room temperature. Under these experimental conditions, parametric optimization of recording parameters has ultimately led to the xenon detection limit of about 0.2 μmol mol^{-1} for 10^4 laser shots. The results show promise for the use of this technique for online monitoring of reactor fuel integrity, and motivate studies for the development of a compact measurement system that could be integrated with the reactor's primary helium-cooling loop.

1 Introduction

Generation IV gas-cooled fast reactors (GCFRs) are receiving significant attention for their increased breeding gain, thermal efficiency, reduced fuel consumption (and thus improved sustainability), and improved operational safety[1]. Helium (He) is often used as a primary coolant since it is chemically inert with relatively favorable heat transfer and transport characteristics. In GCFRs, presence of an appreciable amount of short-lived fission products in the He coolant, such as ^{138}Xe or ^{88}Kr, would provide an early signature of micro-crack formation in the fuel cladding[2]. This motivates the development of online methods for trace detection of fission products and structural materials in He ambient gas, which may be suitable for implementing into instrumentation for next-generation GCFRs. The typical GCFR operating conditions include high temperature (∼850°C) and high pressure (∼13.3 MPa).

Laser-induced breakdown spectroscopy (LIBS) is an optical diagnostic technique that can detect the presence and measure the concentrations of various trace elements in samples or environments of arbitrary composition or phase[3,4]. In LIBS, a high-power laser pulse is focused to ablate and ionize a small volume of the sample to produce a plasma. In fluids (gaseous or liquid environments), depending on the incident intensity and wavelength, nanosecond laser induces the breakdown through multi-photon (MPI) ionization and/or inverse bremsstrahlung (IB). If the MPI is absent, the breakdown develops solely through avalanche ionization after initial IB-driven heating[5,6]. The resulting plasma emission consists of a continuum-, ionic-, atomic-, and, under certain conditions, molecular radiation. The key to successful LIBS analysis of transient plasma emission by optical spectroscopy is determining the optimal period in which the optical signal is collected and analyzed. While not as sensitive as gas chromatography[7], the combination of gas chromatography and mass spectroscopy[8], and laser absorption spectrometry[9], LIBS is more robust and can be readily deployed *in situ*. LIBS has been applied in the past to measuring aerosols[10,11] and trace elements in gaseous mixtures[12–16]. An impact of He presence in enhancing the LIBS analyte signal has been studied for gases[17]. The authors report that He can affect the initial laser-induced gas breakdown through mechanisms such as Penning ionization of gas atoms or molecules in collisions with metastable He atoms but conclude that this effect is less significant than the overall changes in plasma properties. McNaghten *et al.* studied the behavior of He in argon and nitrogen and concluded that the ionization and dissociation of the nitrogen molecule quenches argon emission[14]. Eseller *et al.* investigated the LODs for oxygen, argon, and nitrogen in hydrogen with both gated and non-gated detection[15]. They found that LODs for non-gated optical emission measurements are about four times higher than the ones obtained when the optical emission is gated. In subsequent work, they measured trace concentrations of He (<1%) in a hydrogen gas mixture and reported a LOD value of 78 ppm for He in hydrogen at atmospheric pressure[16]. The difficulty of LIBS measurements in He atmosphere is primarily associated with

[a] *Department of Nuclear Engineering and Radiological Sciences, University of Michigan, Ann Arbor, MI 48109, USA; E-mail: milosb@umich.edu*
[b] *Gérard Mourou Center for Ultrafast Optical Science, University of Michigan, Ann Arbor, MI 48109, USA;*
[c] *Idaho National Laboratory, Idaho Falls, ID 83415, USA.*

its high ionization energy of ~24.6 eV, which requires a high laser intensity in the lens focal region for the breakdown to occur. This, in turn, increases the magnitude of continuum radiation emission, ultimately reducing the sensitivity for trace detection. This is because most measurements are performed at the early stages of the plasma lifetime, when the analyte emission is strong.

Here we assess the baseline performance of the standard LIBS technique for detection of trace amounts of Xe in He-Xe binary mixtures. By optimizing the recording parameters such as detector gate width and delay, we show that μmol mol^{-1}-level sensitivity can be readily achieved. ~~We further discuss the strategies for signal enhancement to achieve sub-ppm detection capability.~~

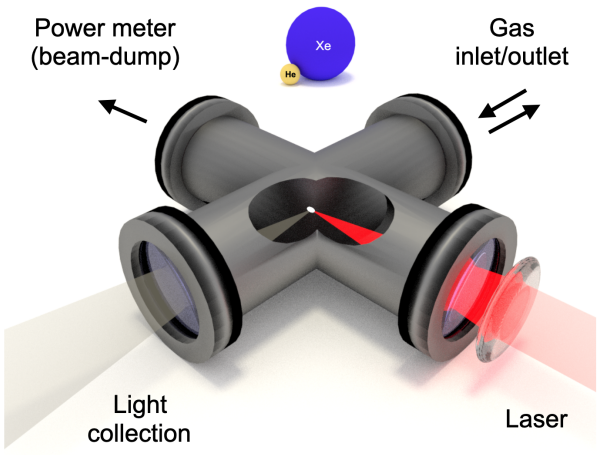

Fig. 1 Gas cell for trace Xe detection in He-Xe mixture following laser-induced breakdown. The difference in gas atom sizes is illustrated by showing their relative scale[18].

2 Experiment

A simplified experimental schematic for trace Xe detection in He-Xe mixture is depicted in Fig. 1. Breakdown of the He-Xe mixture was induced with 1064-nm, 14-ns, 250-mJ pulses from a Nd:YAG laser (Surelite, Continuum) operating at a repetition rate of 10 Hz. The laser beam was focused by a 100-mm focal length lens. The cell was evacuated to the pressure of 10^{-5} Pa (1×10^{-7} mbar) using a turbo pump prior to introducing gas mixtures. Certified He-Xe mixtures of various concentrations (99.999% purity of both constituents) were used for measurements. The trace quantities of Xe are defined as molar fractions (μmol mol^{-1}). The He-only (99.999% pure) background measurements were taken as reference. All experiments were performed under pressure of 1.25 bar (1.25×10^5 Pa). For spectroscopic measurements, plasma emission was collected from a 200-mm distance with a collimator (CC52, Andor) and coupled into a 0.4-mm diameter optical fiber connected to a compact Czerny-Turner spectrograph (MicroHR, 600 lines/mm grating, HORIBA Jobin Yvon). The spectra were recorded by an intensified CCD (iStar T334, Andor) cooled down to -25°C. In order to remove multi-order interference from the near-UV spectral lines, a high-pass filter with a cutoff wavelength of 450 nm was used (FELH0450, ThorLabs). The spectroscopic detection system was wavelength-calibrated with an Ar lamp (Pen Light, Oriel).

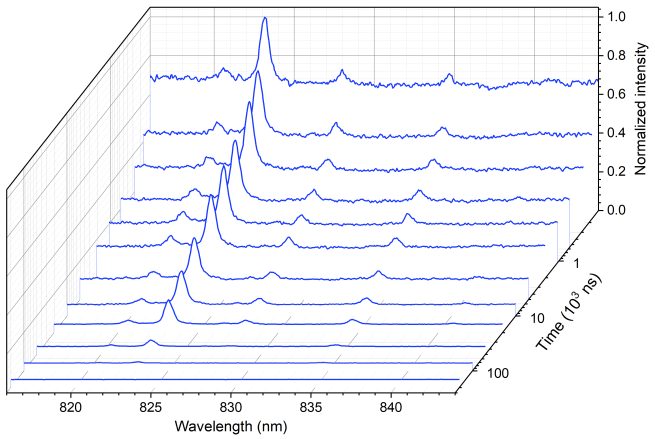

Fig. 2 Temporally resolved emission spectra from He-Xe plasma at 100-µmol mol^{-1} concentration of Xe averaged over 10^3 laser shots.

3 Results and discussion

The near-infrared spectral line of Xe located at 823.16 nm was selected for analytical analysis because of its prominence and absence of spectral interference with He lines. We focus on the spectral region around 823-nm to observe its behavior throughout the plasma lifetime. As a transient radiation source, depending strongly on laser intensity and ambient conditions, laser-produced plasma typically persists up to several tens of microseconds[3,19]. Figure 2 shows that, under the given experimental conditions and 20-μs gate width, the Xe I 823.16-nm line could be observed until at least 100 μs after the laser pulse. This behavior of Xe spectral lines may be associated with the He metastable states in He-Xe binary mixtures[20,21]. The spectral region of interest includes other prominent Xe spectral lines such as Xe I 820.63 nm, Xe I 834.68 nm and Xe I 828.01 nm[22].

One of the limitations of LIBS is its lower sensitivity when compared to several other measurement techniques such as the ones mentioned previously. This is especially pronounced in the early stages of plasma evolution, as the bremsstrahlung contribution to the spectrum reduces the Signal-to-Noise Ratio (SNR) of a chosen spectral line for the analyte. SNR is defined as

$$SNR = \frac{\overline{S}}{\sigma_B}, \quad (1)$$

where $\overline{S}$ is the intensity of the spectral line. The noise level was inferred from the standard deviation of the background (σ_B). The SNR scales inversely with σ_B, defined as

$$\sigma_B = \sqrt{\frac{\sum (X_i - \overline{X})^2}{N}}, \quad (2)$$

where X_i is the individual value of the i-th detector pixel, $\overline{X}$ is the mean value of all pixels within the steady background region 838 nm – 840 nm), and N is the number of pixels. Equation (2) was used to estimate the noise level for SNR calculations. A straightforward method to increase the SNR is to accumulate a

larger number of shots within a given measurement set[23].

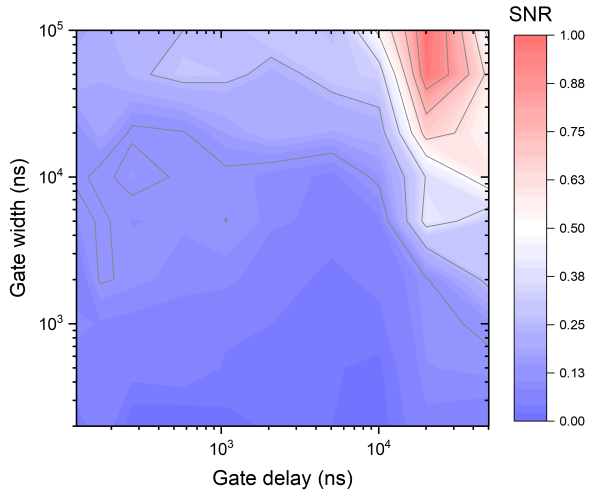

Fig. 3 Normalized signal-to-noise ratio for the Xe I 823.16-nm spectral line in terms of gate width and recording delay.

In order to optimize the SNR, multiple measurements were made, where the gate delay and gate width of the ICCD were varied. The results of these measurements, performed with 100-μmol mol^{-1} Xe concentration and accumulated over 10^3 shots for each pair of gate delay and gate width, are shown in Figure 3. The SNR at early times and short gate widths was reduced by the prominent continuum contribution, favoring the use of relatively long gate delay and width times. A 20-μs gate delay and 100-μs gate width were selected as optimal for subsequent measurements of signal scaling with number of laser shots and detection limit.

For a sufficiently large number of measurements, the SNR can also be expressed as

$$SNR = \alpha N^{\beta}, \quad (3)$$

where α is a fit parameter and β is the best fit power law. The expected value of β is 0.5. An example of the scaling of SNR with the number of measurements (laser shots) is shown in Figure 4 for the 100-μmol mol^{-1} Xe concentration. The nonlinear fit yields β = 0.52, which is in fair agreement with the prediction. The observed scaling for the He-Xe mixture implies that the use of high-repetition-rate (kHz) lasers offers the prospect for significant improvements in sensitivity for trace Xe over the same measurement times.

The spectra of various Xe concentrations after subtraction of He-only reference are presented in Figure 5. Spectra measured at higher Xe concentrations reveal more spectral lines, indicating the presence of higher-lying transitions with upper energy levels above 11 eV (Table 1). As the concentration of Xe decreases, the lines originating from these levels diminish, leaving only the Xe I 823.16-nm observable in the 1-μmol mol^{-1} spectrum.

The calibration curve is constructed based on the five available certified He-Xe mixtures using 10^3 and 10^4 blank-corrected accumulations (Figure 6) and without the use of any normalization technique. It can be seen that the calibration curve experiences saturation at higher concentrations. The saturation becomes prominent approximately at a 1000-μmol mol^{-1} Xe concentration, most likely as a result of self-absorption[24]. A linear fit was constructed for the remainder of the data points. The LOD is determined on the basis of intersection of the linear fit of the area underneath the Voigt line profile and the $3\sigma_B$ noise level. The σ_B value is determined from the spectral linewidth region of the Xe emission line from measurements performed in a He-only environment (analytical blank). In case of 10^3-shot accumulations, we obtain LOD_{1000} = 0.836±0.218, while in the 10^4-shot case we obtain LOD_{10000} = 0.174±0.073. The direct comparison of results obtained using different equipment and in different conditions is often difficult. Nevertheless, we note some typical values that can be found in the literature for gaseous mixtures involving lighter buffer and heavier analyte gas. For example, 17-ppm LOD for Ar was reported in nitrogen ambient, whereas the LOD of 4.9 ppm is expected for Ar in He at 1 bar[14].

The results reported here motivate the work to further improve both sensitivity and the accuracy of LOD measurements, since the required sensitivity for GCFRs lies in the sub-ppm range. There are various strategies to enhance sensitivity of LIBS detection, but

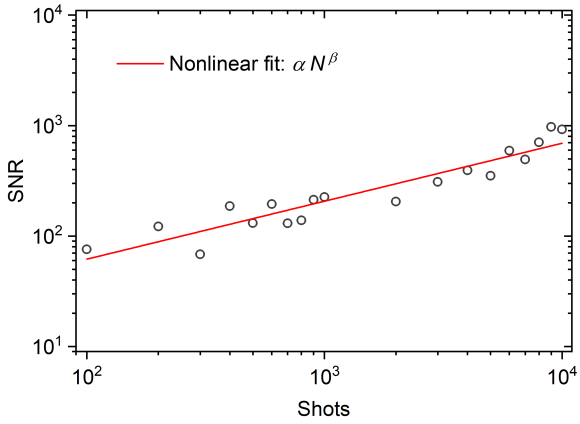

Fig. 4 Scaling of the signal-to-noise ratio for the Xe I 823.16-nm with the number of laser shots at the 100-μmol mol^{-1} Xe concentration.

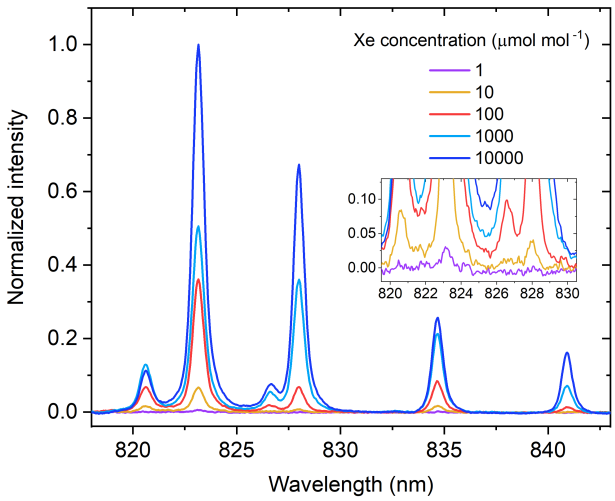

Fig. 5 Typical spectra of He-Xe plasma averaged over 10^4 laser shots at various concentrations and after subtraction of He-only reference spectrum. The inset shows magnified region of interest.

Table 1 Wavelength, transition probability, configuration and term of upper and lower excitation levels of Xe I transitions according to NIST [22].

Species	Wavelength (nm)	Einstein coeff. ($10^6 s^{-1}$)	Lower level Config.	Lower level Term	Upper level Config.	Upper level Term	Lower level energy (eV)	Upper level energy (eV)
Xe I	820.633	20	$5p^5 6s$	$^2P^o_{1/2}$	$5p^5 6p$	$^2P^o_{3/2}$	9.447	10.957
	823.163	28.6	$5p^5 6s$	$^2P^o_{3/2}$	$5p^5 6p$	$^2P^o_{3/2}$	8.315	9.821
	826.652	16.2	$5p^5 6s$	$^2P^o_{1/2}$	$5p^5 6p$	$^2P^o_{1/2}$	9.569	11.069
	828.011	36.9	$5p^5 6s$	$^2P^o_{3/2}$	$5p^5 6p$	$^2P^o_{3/2}$	8.436	9.933
	834.682	42	$5p^5 6s$	$^2P^o_{1/2}$	$5p^5 6p$	$^2P^o_{1/2}$	9.569	11.055
	840.918	3.06	$5p^5 6s$	$^2P^o_{3/2}$	$5p^5 6p$	$^2P^o_{3/2}$	8.315	9.789

we will limit this discussion to the ones applicable to integration with GCFRs. An order-of-magnitude signal enhancement can be achieved through double-pulse excitation [3,24] and/or resonant optical pumping of transitions of interest (combination of LIBS and LIF) [25,26]. Optimization of detection includes light collection with lower f-number, using a detector with higher quantum efficiency, spectrograph with higher light throughput, optics with dedicated antireflection coatings, or simply averaging the signal over more laser shots. With the rapid development of the fiber laser technology, high repetition rate, high peak power, compactness, low cost, and laser robustness are no longer exclusive of each other. A significant technical challenge is related to simulating the working conditions in GCFRs. Experiments at *both* high temperature and high pressure simultaneously are required. The effect of higher temperature may have beneficial effect to the LIBS signal to a certain degree [27,28]. However, keeping in mind that the signal decreases with pressure [29,30], synergistic application of multiple signal-enhancement strategies is necessary to achieve the desired sensitivity in trace Xe detection.

4 Conclusions

In summary, we demonstrated that the optimization of recording parameters in LIBS can result in μmol mol^{-1}-level Xe detection in He-Xe gas mixtures at near atmospheric pressure and room temperature. In order to faithfully reproduce the operating conditions of GCFRs, experiments in a high-temperature and high-pressure environment are needed. Future work will involve mimicking these conditions in a laboratory setting, as well as employing additional signal-enhancement approaches. Based on the present study, LIBS system integration into a He-coolant loop of GCFR is perceived as a viable option for online impurity monitoring. We further note the significance of detection of Xe fission gas in the context of *in-situ* and remote detection for nuclear nonproliferation and nuclear threat reduction applications. For the latter applications it is necessary to examine the potential of LIBS and related techniques to detect Xe in more complex, mixed environments such as air.

Conflicts of interest

There are no conflicts to declare.

Acknowledgements

This work was conducted in conjunction with the Versatile Test Reactor project and is based upon work supported by the U.S. Department of Energy under Prime Contract No. DE-AC07-05ID14517 to the Idaho National Laboratory. Any opinions, findings, and conclusions or recommendations expressed in this publication are preliminary and are those of the author(s) and do not necessarily reflect the views of the U.S. Department of Energy or the Idaho National Laboratory; This work was also supported by the Department of Defense, Defense Threat Reduction Agency (HDTRA1-20-2-0002).

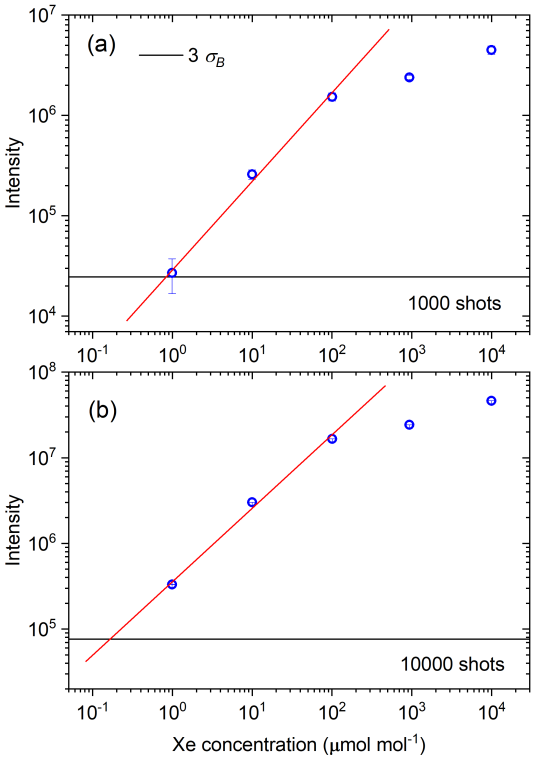

Fig. 6 Calibration plot for Xe with (a) 10^3 and (b) 10^4 accumulated laser shots. The intersection of linear fit with horizontal 3σ-blank line yields the LOD. Most error bars are smaller than the size of the data points.

References

1 G. Lomonaco and W. F. G. van Rooijen, *Science and Technology of Nuclear Installations*, 2009, **2009**, 965757.

2 K. Korsah, P. Ramuhalli, R. Vlim, R. Kisner, C. Britton, D. Wootan, N. Anheier, A. Diaz, E. Hirt, H. Chien, S. Sheen,

S. Bakhtiari, S. Gopalsami, A. Heifetz, S. W. Tam, Y. Park, B. Upadhyaya and A. Stanford, Assessment of Sensor Technologies for Advanced Reactors, 2016.

3 D. A. Cremers and L. J. Radziemski, *Handbook of Laser-Induced Breakdown Spectroscopy*, John Wiley & Sons, NJ, 2013.

4 R. E. Russo, X. Mao, J. J. Gonzalez, V. Zorba and J. Yoo, *Analytical Chemistry*, 2013, **85**, 6162–6177.

5 C. H. Chan, C. D. Moody and W. B. McKnight, *Journal of Applied Physics*, 1973, **44**, 1179–1188.

6 C. H. Chan and C. D. Moody, *Journal of Applied Physics*, 1974, **45**, 1105–1111.

7 J. Havlena, E. J. and K. A. Hutchinson, *Journal of Chromatographic Science*, 1966, **4**, 380–383.

8 Z.-Y. Chen, S.-J. Liu, J.-L. Wang and Y.-Z. Chang, *Chinese Journal of Analytical Chemistry*, 2016, **44**, 468 – 473.

9 P. Jacquet and A. Pailloux, *J. Anal. At. Spectrom.*, 2013, **28**, 1298–1302.

10 G. Gallou, J. B. Sirven, C. Dutouquet, O. L. Bihan and E. Frejafon, *Aerosol Science and Technology*, 2011, **45**, 918–926.

11 M. Boudhib, J. Hermann and C. Dutouquet, *Analytical Chemistry*, 2016, **88**, 4029–4035.

12 C. Haisch, R. Niessner, O. I. Matveev, U. Panne and N. Omenetto, *Fresenius' Journal of Analytical Chemistry*, 1996, **356**, 21–26.

13 V. Sturm and R. Noll, *Appl. Opt.*, 2003, **42**, 6221–6225.

14 E. McNaghten, A. Parkes, B. Griffiths, A. Whitehouse and S. Palanco, *Spectrochimica Acta Part B: Atomic Spectroscopy*, 2009, **64**, 1111 – 1118.

15 K. E. Eseller, F. Y. Yueh and J. P. Singh, *Applied Physics B*, 2011, **102**, 963–969.

16 K. E. Eseller, F.-Y. Yueh, J. P. Singh and N. Melikechi, *Appl. Opt.*, 2012, **51**, B171–B175.

17 C. Henry, P. Diwakar and D. Hahn, *Spectrochimica Acta Part B: Atomic Spectroscopy*, 2007, **62**, 1390 – 1398.

18 E. Clementi, D. L. Raimondi and W. P. Reinhardt, *The Journal of Chemical Physics*, 1967, **47**, 1300–1307.

19 C. G. Parigger, in *Laser-induced breakdown in gases: experiments and simulation*, ed. A. W. Miziolek, V. Palleschi and I. Schechter, Cambridge University Press, 2006, p. 171–193.

20 R. Shuker, A. Szöke, E. Zamir and Y. Binur, *Phys. Rev. A*, 1975, **11**, 1187–1192.

21 R. Shuker, Y. Binur and A. Szöke, *Phys. Rev. A*, 1975, **12**, 515–521.

22 A. Kramida, Y. Ralchenko and J. Reader, *NIST Atomic Spectra Database*, 2020, `http://physics.nist.gov/asd`, National Institute of Standards and Technology, Gaithersburg, MD.

23 Z. Chen, Y. Godwal, Y. Y. Tsui and R. Fedosejevs, *Appl. Opt.*, 2010, **49**, C87–C94.

24 D. W. Hahn and N. Omenetto, *Appl. Spectrosc.*, 2012, **66**, 347–419.

25 R. M. Measures and H. S. Kwong, *Appl. Opt.*, 1979, **18**, 281–286.

26 S. L. Lui, Y. Godwal, M. T. Taschuk, Y. Y. Tsui and R. Fedosejevs, *Analytical Chemistry*, 2008, **80**, 1995–2000.

27 W. Xu, A. Chen, Q. Wang, D. Zhang, S. Li, Y. Jiang, X. Gao and M. Jin, *J. Anal. At. Spectrom.*, 2019, **34**, 2288–2294.

28 R. Hai, Z. He, D. Wu, W. Tong, H. Sattar, M. Imran and H. Ding, *J. Anal. At. Spectrom.*, 2019, **34**, 2378–2384.

29 M. Noda, Y. Deguchi, S. Iwasaki and N. Yoshikawa, *Spectrochimica Acta Part B: Atomic Spectroscopy*, 2002, **57**, 701 – 709.

30 E. Vors, C. Gallou and L. Salmon, *Spectrochimica Acta Part B: Atomic Spectroscopy*, 2008, **63**, 1198 – 1204.